# sReactivation of $CeO_2$-based Catalysts in the HCl Oxidation Reaction: *In situ* Quantification of the Degree of Chlorination and Kinetic Modeling

Yu Sun,[a, b] Franziska Hess,[c, d] Igor Djerdj,[e] Zheng Wang,[a, b] Tim Weber,[b, f] Yanglong Guo,*[a] Bernd M. Smarsly,*[b, f] and Herbert Over*[b, f]

Deactivation of $CeO_2$-based catalysts in the HCl oxidation reaction proceeds via selective bulk chlorination of the active $CeO_2$ component to form $CeCl_3 \times nH_2O$. We study the reactivation of two bulk-chlorinated $CeO_2$-based Deacon catalysts by oxygen treatment at 430 °C, namely pure $CeO_2$ and 20 mol% of $CeO_2$ supported on preformed $ZrO_2$ particles ($20CeO_2@ZrO_2$), with a dedicated experiment. In the flow reactor setup we determine *in-situ* the degree of chlorination of the catalyst by quantifying down-stream with in-situ UV-Vis spectroscopy the total amount of chlorine in the catalyst that is exchanged by reoxidation at 430 °C. The activity of deactivated $20CeO_2@ZrO_2$ can be fully restored by oxygen exposure at 430 °C, while that of pure $CeO_2$ declines steadily. Since the UV-Vis analytics is fast and sensitive, we can follow the kinetics of reoxidation. To rationalize the observed kinetics, we develop a modified Johnson-Mehl-Avrami-Kolmogorov (JMAK) model based on a nucleation-and-growth approach for the reoxidation of the catalyst starting from the chlorinated phase. The fast reoxidation kinetics of chlorinated $20CeO_2@ZrO_2$ is traced to a fast nucleation rate.

## 1. Introduction

Catalyst stability is a severe concern in heterogeneous catalysis[1] and many ways of catalyst deactivation have been reported in literature,[2] among which most studies have focused on sintering of the active component with the consequence of a reduction of the active surface area. However, there is a class of catalysts that undergoes chemical transformation under reaction conditions accompanied by a deterioration of catalytic performance. This kind of reaction-induced catalyst transformation is for instance encountered with the HCl oxidation reaction, the so-called Deacon process [Eq. (1)],[3,4] which is employed to recover chlorine from the omnipresent byproduct HCl in many industrial processes:

$$4HCl + O_2 \rightarrow 2H_2O + 2Cl_2; \quad \Delta_r H = -114\,kJ/mol \tag{1}$$

For the Deacon process, low stability of the catalyst has been an ongoing problem that had deferred its industrial commercialization by 130 years. For instance, the original catalyst CuO, invented by Deacon 1868, readily undergoes bulk chlorination towards $CuCl_2$. Since $CuCl_2$ is volatile at a reaction temperature above 400 °C, the catalyst is gradually lost during operation. Only in the year 2000 Sumitomo Chemical commercialized an active and stable Deacon catalyst based on $RuO_2$ that is supported on rutile $TiO_2$.[5]

Already very early, the catalyzed HCl oxidation over oxide surface was envisioned to be composed of a reduction step by HCl followed by a reoxidation step of the chlorinated oxide by

[a] Y. Sun, Z. Wang, Prof. Y. Guo
Key Laboratory for Advanced Materials
Research Institute of Industrial Catalysis
East China University of Science and Technology
Shanghai 200237 (P.R. China)
E-mail: ylguo@ecust.edu.cn
[b] Y. Sun, Z. Wang, T. Weber, Prof. B. M. Smarsly, Prof. H. Over
Physikalisch-Chemisches Institut
Justus Liebig Universität
Heinrich-Buff-Ring 17
35392 GießenGiessen (Germany)
E-mail: Bernd.Smarsly@phys.chemie.uni-giessen.de
Herbert.Over@phys.chemie.uni-giessen.de
[c] Prof. F. Hess
Institute of Physical Chemistry
RWTH Aachen
Landoltweg 2
52074 Aachen (Germany)
[d] Prof. F. Hess
Institut für Chemie
Technische Universitaet Berlin
Strasse des 17. Juni 124
10623 Berlin (Germany)
[e] Prof. I. Djerdj
Department of Chemistry
J. J. Strossmayer University of Osijek
Ulica cara Hadrijana 8/a
HR-31000 Osijek (Croatia)
[f] T. Weber, Prof. B. M. Smarsly, Prof. H. Over
Zentrum für Materialforschung
Justus Liebig Universität
Heinrich-Buff-Ring 16
35392 Giessen (Germany)

Supporting information for this article is available on the WWW under https://doi.org/10.1002/cctc.202000907

molecular oxygen.[6] For the commercialized $RuO_2$/rutile-$TiO_2$ catalyst these reduction and oxidation steps are not bulk transformations of the catalysts, but rather take place at the surface only.[7] However, for the case of $CeO_2$-based catalysts, a promising and viable alternative to $RuO_2$, it was recognized that they deactivate in the Deacon reaction through bulk chlorination,[8–12] although being partly reactivated with excess oxygen in the reaction feed at reaction temperatures of typically 430 °C.[8,13,14] Improved chemical stability against bulk chlorination is achieved by mixing $CeO_2$ with $ZrO_2$, either in the form of solid solutions[15,16] or as $CeO_2$ deposited on preformed $ZrO_2$ particles.[17,18] The degree of chlorination that is directly correlated to the deactivation of the catalyst can be quantified in-situ by prompt gamma activation analysis (PGAA),[13,19] but also ex-situ either by thermogravimetric analysis (TGA-MS)[8] or by quantitative X-ray diffraction (XRD: Rietveld refinement).[9,18]

Here, we report a dedicated experiment for quantifying the degree of chlorination of the $CeO_2$-based catalyst in the very same reactor with which also the catalytic Deacon tests are performed. With this unique experiment, we can readily follow *in-situ* the kinetics of its reactivation via reoxidation. We exemplify this method as a proof-of-principle experiment with two Deacon powder catalysts, one is pure $CeO_2$ and the other is 20 mol% $CeO_2$ supported on preformed $ZrO_2$ particles ($20CeO_2@ZrO_2$). It turns out that the activity of pure $CeO_2$ is not fully recovered after reoxidation of the previously bulk-chlorinated sample. However, the activity of $20CeO_2@ZrO_2$ is quantitatively recovered after the second reactivation cycle. In addition, the reoxidation of $20CeO_2@ZrO_2$ is much faster compared to that of pure $CeO_2$. In a phenomenological kinetic model based on a nucleation-and-growth approach, we can describe the faster reoxidation of the supported catalyst by a higher nucleation rate due to the support ($ZrO_2$) surface.

## Experimental Section

### Experimental Details

The Deacon reaction was conducted in a custom fixed-bed flow reactor.[20] The reactor comprises the gas supply, the quartz tube reactor, heated by a computer-controlled furnace, and UV/vis analytics (Ocean Optics USB4000 with a DH-2000-BAL light source) for chlorine quantification. The following gases were used in the reaction measurements: HCl (99.995%), $O_2$ (99.999%) and Ar (99.999%) from AirLiquide, and the flow rate of gases was controlled by digital mass flow controllers (MKS Instruments 1179B). Prior to feeding the gas mixture into the reactor, Ar was dried using a water absorption cartridge (ALPHAGAZTM purifier $H_2O$-free, AirLiquide). The absorbance at a wavelength of $\lambda_{max} = 329$ nm (absorption maximum of chlorine) is proportional to the chlorine space time yield (STY) that is defined as the molar amount of product per time and mass catalyst.

Besides catalytic activity tests, the flow reactor with the UV-Vis analytics can be employed to quantify the degree of chlorination of the catalyst after Deacon reaction. In doing so we reoxidized the chlorinated catalysts by oxygen exposure and the replaced chlorine from the catalyst is quantified by UV-Vis spectroscopy. Since the sensitivity of the UV-Vis spectroscopy is high and the data acquisition is fast enough, this dechlorination process of the once (partly) chlorinated catalyst can be followed in-situ as a function of time. Iodometry is employed to calibrate the extinction in the UV-Vis signal to absolute $Cl_2$ concentrations. The detailed calibration steps are shown in **Section 1.3** of the Supporting Material.

The proposed method for quantifying the degree of catalyst chlorination is *in situ*. In particular, we developed a reliable measurement protocol that is summarized in Figure 1 with the total flow set to 15 $cm^3$ STP$min^{-1}$ (sccm) and the catalyst kept at 430 °C. Each reaction step is followed by a purging step with pure Ar to remove the weakly held species from the reactor walls until the baseline of the chlorine UV-Vis signal is stable. The Deacon reaction experiments is first carried out under so-called "mild" condition with the reaction feed $Ar:HCl:O_2 = 10.5:1.5:3$. After the catalytic activity has reached steady state, the activity in terms of space time yield (STY) can be determined. Subsequently pure Ar is purged and the deactivation experiment is performed under so-called "harsh" condition with a feed ratio of $Ar:HCl:O_2 = 9:4.5:1.5$. When the catalyst is fully deactivated due to in-depth chlorination, pure Ar is purged. To quantify the degree of chlorination, the deactivated $CeO_2$-based catalyst is exposed to 50 vol.% $O_2$ (balanced by argon) for 5 h at the reaction temperature until the deactivated catalyst is fully reoxidized. During reactivation, oxygen replaces chlorine in the catalyst, and the replaced chlorine can be quantified by UV-Vis spectroscopy. After completion of the reactivation step, the reactor is purged with Ar. This terminates the first deactivation/reactivation cycle. The deactivation/reactivation cycle is repeated twice in order to estimate the activity loss due to restoration.

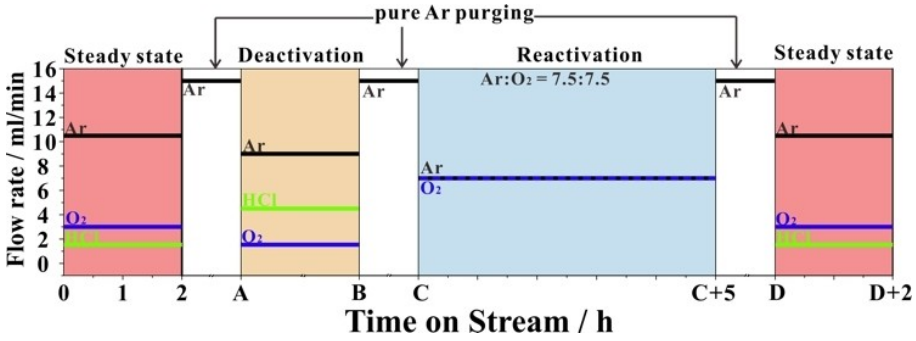


**Figure 1.** The measurement protocol (reaction feed composition) for determining the degree of chlorination of a $CeO_2$-based catalyst after full deactivation. The total flow rate is always 15 sccm and the catalyst is kept at 430 °C. Steady state activity experiments are performed before and after restoration (reactivation).

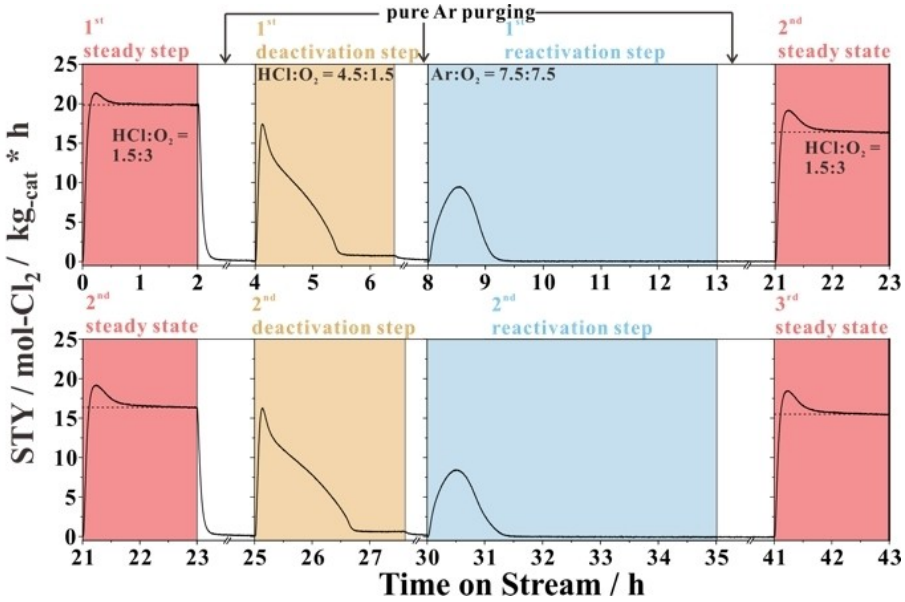


**Figure 2.** Chlorine evolution of pure $CeO_2$ under the HCl oxidation reaction at $T = 430\,^{\circ}C$, total flow rate15 sccm, 26 mg catalyst as a function of time on stream under varying reaction conditions provided by the measurement protocol (cycle) of Figure 1. The cycle was carried out twice to compare the steady state activity (dashed red line) dependent on the restoration cycle.

Further details about catalyst preparation and the employed characterization methods can be found in the **Section 1** of the Supporting Material.

### Computational Details

During the reactivation step described in **Experimental Details**, we monitor the reoxidation kinetics through the evolution of $Cl_2$ as a function of time. We employ a phenomenological approach to model the differences between the reoxidation kinetics of the samples. We first note that the measured $Cl_2$ signal during reoxidation released by the reaction [Eq. (2)].

$$CeCl_3 + O_2 \rightarrow CeO_2 + \frac{3}{2}Cl_2 \tag{2}$$

represents the derivative of the fraction of the transformed phase ($CeO_2$), denoted as $\varepsilon$, over time, $t$: $x_{Cl_2}(t) = \frac{d\varepsilon}{dt}$, i.e., the rate of the phase transformation. The fraction of transformed phase as a function time $\varepsilon(t)$ can therefore be obtained by the numerical integral of the $Cl_2$ signal over time. All our reoxidation signals (e.g., the blue area in Figure 2) have a characteristic shape where the initial rate of transformation is zero, goes through a maximum and then gradually returns to zero. The integral of the $Cl_2$ signal over time is a sigmoidal function. This behavior suggests a self-accelerating process, which is typical for a nucleation and growth mechanism. Since the phase transformation requires the formation of nuclei of the new phase, the initial growth rate is zero if no nuclei have been formed previously.

The kinetics of such a phase transition can be described using the Johnson-Mehl-Avrami-Kolmogorov (JMAK) approach. The JMAK theory assumes that nucleation occurs randomly at a constant rate per sample volume. Nucleation in the JMAK theory can proceed either spontaneously from an oversaturated (or undercooled) vapor or aided by solid surfaces. As the existence of a supersaturated vapor is highly unlikely in a flow reactor, we assume that available surfaces of catalyst support ($SiO_2$ and $ZrO_2$) and untransformed materials ($CeO_2$, $CeCl_3$) serve as heterogeneous nucleation sites for $CeO_2$ during reoxidation. However, we note that the JMAK theory cannot distinguish between nucleation mechanisms, and different nucleation mechanisms will only be reflected in different nucleation rates. The nuclei then grow at a constant rate until the whole sample volume is transformed. The transformed dimensionless volume fraction $\varepsilon_B = \frac{V_B}{V_{tot}}$ of phase B ($CeO_2$) as a function of time can be expressed by the well-known Avrami equation [Eq. (3)].

$$\varepsilon_B(t) = 1 - e^{-k_{eff}\, t^{m+1}}, \tag{3}$$

where $k_{eff}$ is an effective rate constant and $m$ is the order of the growth process, with the integer values 1, 2, 3 corresponding to 1D, 2D and 3D growth.

As will be shown in Sections 3.1 and 3.2 our system does not fulfill some of the assumptions made in the derivation of the standard Avrami equation: (1) Our catalyst does not undergo a pure phase transition. Rather it is a phase transformation due to a chemical reaction of $CeCl_3$ with $O_2$. (2) The catalyst bed contains some untransformed oxide at the start of the reoxidation reaction, which means that the number of nuclei and the volume fraction of oxidized phase are not zero initially. (3) Our supported sample grows as a layer on top of $ZrO_2$, which contains approximately 25% of the supported $CeO_2$ in $20CeO_2@ZrO_2$. The remaining 75% form $CeO_2$ particles. The sample therefore must expose two different growth modes, possibly with different rates. (4) The detected $Cl_2$ signal represents the derivative of the transformed volume fraction with respect to time, $\frac{d\varepsilon_B}{dt}$. Therefore, we derive a modified JMAK model in the supporting material that accounts for these additional features, whose derivation is shown in detail in Section 2 of the supporting information. Denoting $n_{nuc}$ as the number of nuclei, $r$ as the radius and $\varepsilon_{CeO_2}$ as the volume fraction of $CeO_2$, we finally arrive at three coupled differential equations [Eqs. (4)–(6)].

$$\frac{dn_{nuc}}{dt} = k_{nuc} \cdot p(O_2)(t), \tag{4}$$

$$\frac{dr}{dt} = k_{grow} \cdot p(O_2)(t), \tag{5}$$

$$\frac{d\varepsilon_{CeO_2}}{dt} = n_{nuc}(t) \cdot \left(1 - \varepsilon_{CeO_2}(t)\right) \cdot \left(\frac{1}{m\Gamma\left(\frac{m}{2}\right)} \cdot 2\,\pi^{\frac{m}{2}} \cdot r(t)^{m-1}\right). \tag{6}$$

Here $t$, $k_{nuc}$ and $k_{grow}$ represent time and the rate constants. The $\left(\frac{1}{m\Gamma\left(\frac{m}{2}\right)} \cdot 2\,\pi^{\frac{m}{2}} \cdot r(t)^{m-1}\right)$ term in Equation (6) describes the surface area of an $m$-dimensional sphere, where $\Gamma(z)$ is the gamma function (please see Section 2 in the Supporting Material for full details). Since the switching of gas in our reactor is not instantaneous, we approximate the time-dependence of the $O_2$ partial pressure with a sigmoid function to account for the transition between Ar and $O_2$ atmosphere [Eq. (7)]:

$$p(O_2)(t) = p_\infty(O_2) \cdot \frac{t_s \cdot t}{1 + |t_s \cdot t|}. \tag{7}$$

From the known relaxation behavior of our flow reactor we estimate that $t_s = 50\ h^{-1}$, which means that switching is complete after about 15 minutes. In our experimental protocol $p_\infty(O_2) = 0.5$ bar during the reoxidation step. The coupled differential equations are solved numerically and the parameters $k_{nuc}$, $k_{grow}$ and $m$ are fitted to the experimental reoxidation data as a single data set using a least-squares approach. We employ a squared residual $\bar{S}$ that is averaged over the four experiments [Eq. (8)]:

$$\bar{S} = \frac{\sum_{i=1}^{4} w_i S_i}{\sum_{i=1}^{4} w_i}, \tag{8}$$

where $S_i$ and $w_i$ are the squared residual and weight of experiment $i$.

The squared residual $S_i$ is defined as the squared difference between the fitted signal $\hat{y}_{i,j}$ and measured signal $y_{i,j}$, summed over all data points $j$ [Eq. (9)]:

$$S_i = \sum_j \left(\hat{y}_{i,j} - y_{i,j}\right)^2 \tag{9}$$

We thereby fit all experiments simultaneously, employing the same $k_{grow}$ and $m$ for both samples. We employ different $k_{nuc}$ for the two samples. Altogether, four parameters are fitted to the experimental data.

## 2. Results and Discussion

### 2.1. Reactivation of the bulk-chlorinated $CeO_2$-based catalyst in the HCl oxidation reaction

We conduct two cycles of deactivation/reactivation for pure $CeO_2$ catalyst under the HCl oxidation reaction at T = 430 °C as summarized in Figure 2. Firstly, we measure the steady state activity of the $CeO_2$ catalyst under mild condition (Ar:HCl:$O_2$ = 10.5:1.5:3) with the STY being 20 $mol_{Cl2}\,kg_{cat}^{-1}\,h^{-1}$. After Ar purging, the catalyst is exposed to a harsh reaction mixture (Ar:HCl:$O_2$ = 9:4.5:1.5). During 1.5 h on stream, the STY of $CeO_2$ declines continuously and saturates finally at a residual activity that is likely due to hydrated $CeCl_3$.[11,18] In the next step, the deactivated $CeO_2$ catalyst is reactivated by the mixed atmosphere of $O_2$ and Ar (Ar:$O_2$ = 7.5:7.5). The broad chlorine peak is attributed to the chlorine signal that is formed by the oxidation of $CeCl_3 \times nH_2O$. This reactivation step takes about 1.4 h. With the assumed reaction of Equation (2), we can determine the chlorination degree, defined as $n(CeCl_3)/(n(CeCl_3) + n(CeO_2))$, of the deactivated $CeO_2$ sample: The integrated chlorine peak area is 6.7 $mol_{Cl2}\,kg_{cat}^{-1}$, combined with the catalyst amount of 26 mg and molar mass of 172.1 g/mol of $CeO_2$, that results in a chlorination degree of 75 ± 3% for the fully-deactivated $CeO_2$ catalyst.

Consistent with literature[13] $CeO_2$ is found to be not fully transformed to hydrated $CeCl_3$. Last, we measure again the steady state activity under mild reaction condition that turns out to be 16.4 $mol_{Cl2}\,kg_{cat}^{-1}\,h^{-1}$ and is hence 17% lower than that of the fresh one.

Subsequently, we repeat the deactivation/reactivation cycle. The pure $CeO_2$ catalyst under harsh reaction condition fully deactivates after 1.7 h on stream. The replaced chlorine amount of 6.3 $mol_{Cl2}\,kg_{cat}^{-1}$ translates to a chlorination degree of 68 ± 4%, which is slightly lower than after the first deactivation. The activity of the $CeO_2$ catalyst after the second reactivation is 15.4 $mol_{Cl2}\,kg_{cat}^{-1}\,h^{-1}$, that is 6% lower than after the first and 23% lower than the initial activity.

In summary, we observe that the deactivated $CeO_2$ catalyst can be restored by reoxidation with pure oxygen, but the steady state activity declines steadily after each restoration step. The decline in chlorination degree may be traced to the formation of larger $CeO_2$ particles as will be shown in the following section.

In Figure 3, we summarize the same deactivation/reactivation series and evaluation procedure for the $20CeO_2@ZrO_2$ catalyst. For the $20CeO_2@ZrO_2$ sample 20 mol% $CeO_2$ is coated on preformed $ZrO_2$ particles, forming a covering ultrathin $CeO_2$ layer (5 mol% and 1.6 ± 0.2 nm thick) together with adhering $CeO_2$ particles (15 mol%).[18] The activity of the fresh $20CeO_2@ZrO_2$ catalyst under mild condition is 20.2 $mol_{Cl2}\,kg_{cat}^{-1}\,h^{-1}$. When switching to harsh reaction conditions, the STY of $20CeO_2@ZrO_2$ drops until it has saturated after 7 h on stream with a residual activity that is likely due to $ZrO_2$ and $CeCl_3 \times nH_2O$. Next, the deactivated $20CeO_2@ZrO_2$ catalyst is fully recovered by exposure to $O_2$ at 430 °C. In this reactivation step, the reoxidation of $20CeO_2@ZrO_2$ is completed after 0.4 h and is hence substantially faster than the reoxidation of the pure $CeO_2$ catalyst. The integrated chlorine peak contains 2.3 $mol_{Cl2}\,kg_{cat}^{-1}$. Combined with the amount (30.3 mg) and molar mass (132.8 g/mol) of $20CeO_2@ZrO_2$, this implies a chlorination degree of 100% for fully deactivated $20CeO_2@ZrO_2$.

The activity of reactivated $20CeO_2@ZrO_2$ under mild condition is 18.5 $mol_{Cl2}\,kg_{cat}^{-1}\,h^{-1}$, 8% lower than that of the fresh

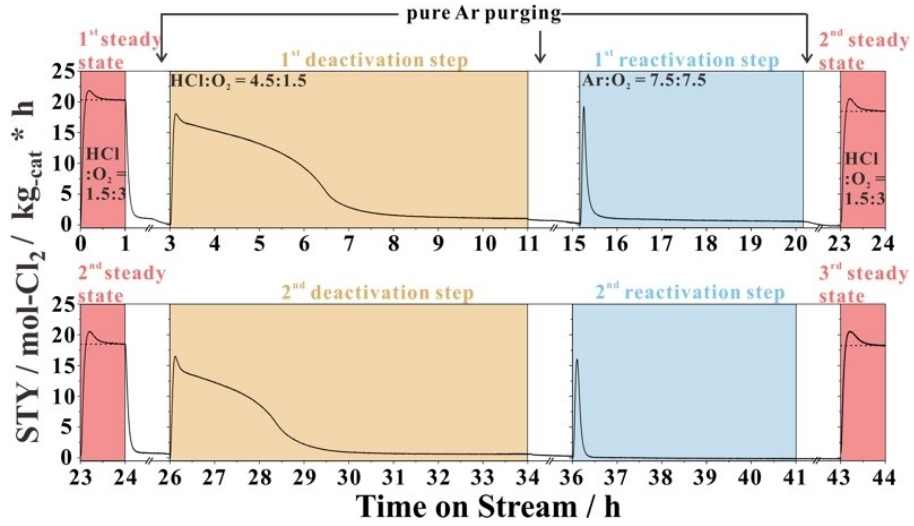


**Figure 3.** Chlorine evolution of $20CeO_2@ZrO_2$ under the HCl oxidation reaction at T = 430 °C, total flow rate15 sccm, 30 mg catalyst as a function of time on stream under varying reaction conditions provided by the measurement protocol (cycle) of Figure 1. The cycle was repeated twice to compare the steady state activity (dashed red line) dependent on the restoration cycle.

one. In the next deactivation/reactivation cycle, the chlorine peak area due to oxygen replacement contains 2 $mol_{Cl2}\,kg_{cat}^{-1}$, leading to a chlorination degree of 91 ± 2%. We finally evaluate the activity of $20CeO_2@ZrO_2$ after the second reactivation step to be 18.3 $mol_{Cl2}\,kg_{cat}^{-1}\,h^{-1}$ which is practically identical to that of $20CeO_2@ZrO_2$ catalyst after the first reactivation.

### 2.2. Characterization of the fresh, deactivated and reactivated $CeO_2$-based catalysts

The structures of the fresh, deactivated and reactivated $CeO_2$ and $20CeO_2@ZrO_2$ catalysts were thoroughly characterized by XRD (Figure 4a). The observed reflections of the fresh $CeO_2$ sample belong to the cubic fluorite structure (ICDD NO. 00–034-0394). The $CeCl_3 \times nH_2O$ reflections are detected for the deactivated $CeO_2$ sample, clearly evidencing bulk chlorination and thus explaining the rapid deactivation of the pure $CeO_2$ sample. As summarized in Table 2, Rietveld refinement of XRD data of deactivated $CeO_2$ sample shows that 76% of the pure $CeO_2$ sample is transformed to $CeCl_3 \times 7H_2O$. This result agrees remarkably well with the fraction of hydrated $CeCl_3$ determined from UV-Vis quantification of the dechlorination peak, providing 77% of $CeCl_3$ for the pure $CeO_2$ sample. Interestingly, the crystallite size of $CeO_2$ in the deactivated $CeO_2$ sample (19 nm) is larger than the initial crystallite size (10 nm). Our interpretation of these results from Rietveld refinement is that small $CeO_2$ particles are completely transformed to $CeCl_3 \times 7H_2O$ upon

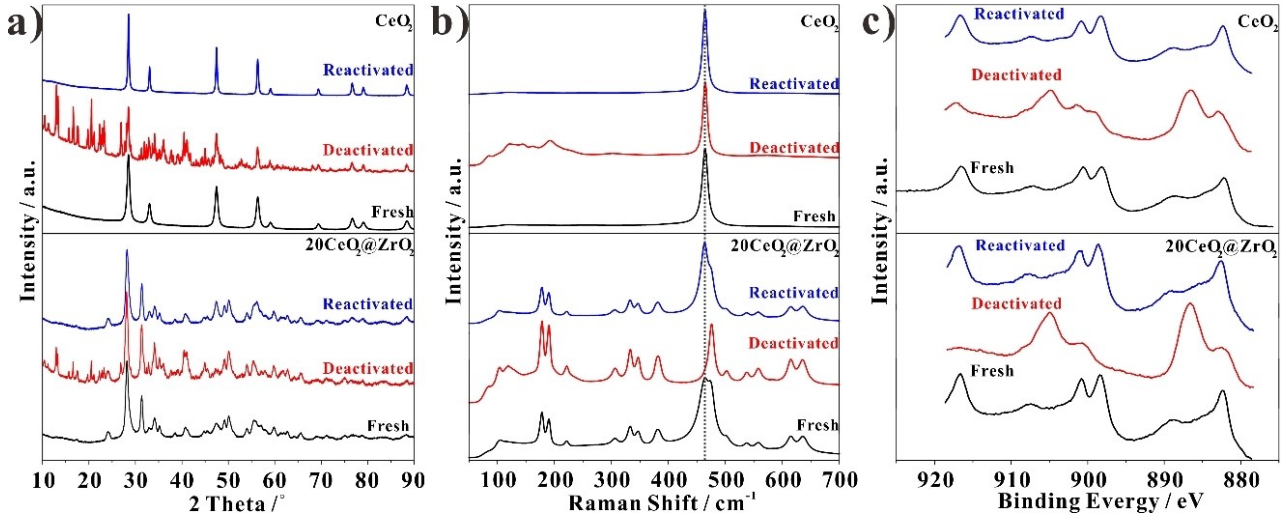


**Figure 4. a)** XRD patterns, **b)** Raman spectra and **c)** Ce 3d XPS of fresh (black), deactivated (red) and reactivated (blue) $CeO_2$ (top panel) and $20CeO_2@ZrO_2$ (bottom panel)

chlorination. Only larger particles remain partly as $CeO_2$ after chlorination, thus increasing the average size of $CeO_2$ crystallites. The XRD pattern of reactivated $CeO_2$ is attributed to a cubic fluorite structure. The width of the reflections of the reactivated sample (Figure 4a: top, blue) has visibly decreased compared to the fresh sample (Figure 4a: top, black). Consistently, we obtain an average crystallite size of around 25 nm for the reactivated $CeO_2$ sample, substantially larger than the fresh one (10 nm; Table 1). This increase in particle size explains the observed activity loss of the reactivated $CeO_2$ sample.

The XRD pattern of the fresh $20CeO_2@ZrO_2$ catalyst (Figure 4a: bottom) consists of a superposition of the cubic phase of $CeO_2$ (ICDD NO. 00–034-0394) and the monoclinic phase of $ZrO_2$ (ICDD NO. 00–036-0420). For the deactivated $20CeO_2@ZrO_2$ sample, the $CeCl_3 \times nH_2O$ concentration is determined to be 21 mol% in agreement with the nominal percentage of 20 mol% $CeO_2$ and therefore results in a degree of chlorination of 100%. The reactivated $20CeO_2@ZrO_2$ sample exhibits in XRD a superposition of the cubic phase of $CeO_2$ and of the monoclinic phase of $ZrO_2$ with a crystallite size of $CeO_2$ of around 7.8 nm (Table 1), slightly increased with respect to the fresh sample (6.5 nm, Table 1).

In Figure 4b we summarize the corresponding Raman experiments of fresh, deactivated and reactivated $CeO_2$ and $20CeO_2@ZrO_2$. The Raman spectrum of fresh $CeO_2$ is dominated by a strong band at 464 $cm^{-1}$ that corresponds to the $F_{2g}$ mode (Ce–O–Ce vibration) of the $CeO_2$ fluorite phase.[21,22] The Raman spectrum of deactivated $CeO_2$ exhibits an additional feature at 119 $cm^{-1}$ that belongs to pure $CeCl_3 \times nH_2O$.[18] Therefore, Raman spectroscopy evidences bulk chlorination in agreement with the XRD results in Figure 4a. The reactivated sample shows only a strong Raman band at 464 $cm^{-1}$, thus indicating a complete transformation to the $CeO_2$ fluorite structure.

The double feature at 470 $cm^{-1}$ of $20CeO_2@ZrO_2$ indicates the coexistence of $CeO_2$ (fluorite structure) and $ZrO_2$ (with monoclinic structure) (Figure 4b). The Raman spectrum of the deactivated $20CeO_2@ZrO_2$ also exhibits an additional feature at 119 $cm^{-1}$, while the $CeO_2$-related contribution at 464 $cm^{-1}$ disappears. This is clear evidence that all the $CeO_2$ species have been transformed to hydrated $CeCl_3$ after harsh Deacon reaction. The Raman spectrum of the reactivated sample reveals a stronger ceria peak intensity than the fresh one, indicating that ceria particles have grown in size after the reactivation step fully consistent with XRD experiments in Figure 4a.

In Figure 4c, we compile X-ray photoemission (XP) spectra of fresh, deactivated and reactivated $CeO_2$ and $20CeO_2@ZrO_2$. Compared to the fresh $CeO_2$, the XP spectrum of the deactivated $CeO_2$ shows the superposition of $CeCl_3$, $Ce_2O_3$ and $CeO_2$ signals,[23,24] suggesting that the $CeO_2$ has not been fully chlorinated under harsh Deacon condition, which is compatible with the Rietveld refinement of the XRD data. From XPS the chlorination degree turned out to be 64% (Table 2); the detailed fitting of XP spectra can be found in Figure S3. The XPS of reactivated $CeO_2$ is practically identical to that of the fresh sample that is indicative of a full recovery of the catalyst.

Fresh $20CeO_2@ZrO_2$ exhibits a similar Ce 3d XP spectrum as the pure $CeO_2$, while that of the deactivated $20CeO_2@ZrO_2$ catalyst comprises only features of $CeCl_3 \times nH_2O$ consistent with the XRD quantification result. The Ce-3d spectrum of the reactivated sample is identical to the fresh one. However, the effective ceria concentration of the reactivated sample decreases from 53% to 41% (Table 2) which means that the ceria particles have partially agglomerated into larger adhering particles. Since XPS is surface-sensitive and the surface-to-volume ratio has decreased upon sintering, the Ce 3d signal intensity declines.

The TEM (Transmission electron microscopy) images and XEDS (X-ray energy dispersive spectroscopy) mappings of deactivated $20CeO_2@ZrO_2$ in Figures 5a, b indicate a uniform distribution of Ce (blue) and Cl (yellow) across the $ZrO_2$ particles (green). Together with the low catalytic activity of hydrated $CeCl_3$ (cf. Figure 3) we conclude that the hydrated $CeCl_3$ is highly dispersed over the $ZrO_2$ particles after chlorination. The TEM images of the reactivated sample (Figures 5c, d) reveal that both the adhering thin $CeO_2$ layer and the $CeO_2$ particle on $ZrO_2$ particle structures have been recovered after oxygen treatment at 430 °C. The TEM micrographs and the XEDS mappings look similar to those of the fresh sample (Figure S4), in accordance with the full recovery of the activity.

**Table 1.** Crystallite size and BET surface area of fresh, deactivated and reactivated $CeO_2$, $20CeO_2@ZrO_2$ catalysts. Catalytic activity of fresh and reactivated $CeO_2$, $20CeO_2@ZrO_2$ catalysts.

| Samples | Crystalline Size [nm] [a] | | | Surface area [$m^2/g$] [b] | STY [mol-$Cl_2$/$kg_{-cat}$ h] [c] |
|---|---|---|---|---|---|
| | $CeO_2$ | $CeCl_3 \times nH_2O$ | $ZrO_2$ | | |
| $CeO_2$ | 10 | n.a. | n.a. | 46 | 20.0 |
| Deactivated $CeO_2$ | 19 | 11($6H_2O$)/ 62($7H_2O$) | n.a. | – | |
| Reactivated $CeO_2$ | 25 | n.a. | n.a. | 26 | 16.4; 15.4[d] |
| $20CeO_2@ZrO_2$ | 6.5 | n.a. | 12 | 46 | 20.2 |
| Deactivated $20CeO_2@ZrO_2$ | – | 39($7H_2O$) | 12 | – | |
| Reactivated $20CeO_2@ZrO_2$ | 7.8 | n.a. | 13 | 33 | 18.5; 18.3[d] |

[a] Determined by Rietveld refinement. [b] Determined by BET method. [c] Determined by fixed-bed flow reactor. [d] STY after first and second reactivation.

**Table 2.** The concentration of $CeO_2$, $CeCl_3$ of fresh, deactivated and reactivated $CeO_2$, $20CeO_2@ZrO_2$ catalysts.

| Samples | $CeO_2$ content [mol%] [a] | Chlorination degree [%] | | Surface atomic concentration [b] | |
|---|---|---|---|---|---|
| | | [a] | [b] | Ce/ (Ce + Zr) | Cl/ (Ce + Zr) |
| $CeO_2$ | n.a. | n.a. | n.a. | 100% | n.a. |
| Deactivated $CeO_2$ | n.a. | 76% | 64% | 100% | 190% |
| Reactivated $CeO_2$ | n.a. | n.a. | n.a. | 100% | n.a. |
| $20CeO_2@ZrO_2$ | 16.4 | n.a. | n.a. | 53% | n.a. |
| Deactivate $20CeO_2@ZrO_2$ | n.a. | 100% | 100% | 31% | 100% |
| Reactivated $20CeO_2@ZrO_2$ | 23 | n.a. | n.a. | 41% | n.a. |

[a] Determined by Rietveld refinement. [b] determined by XPS.

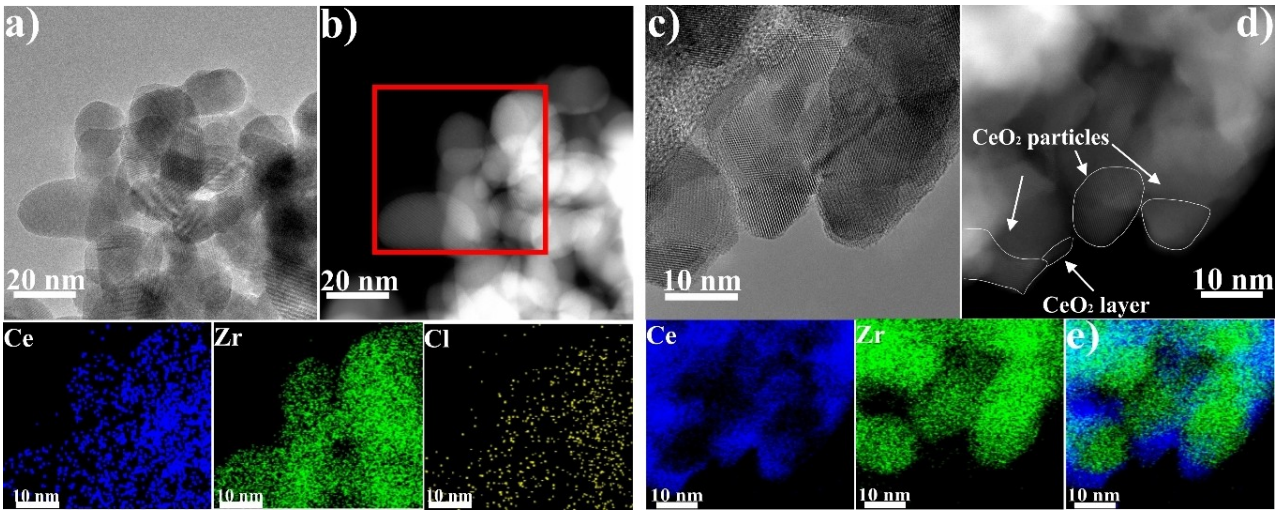


**Figure 5.** Aberration-Corrected High-Resolution TEM images of **a)** fully deactivated and **c)** reactivated $20CeO_2@ZrO_2$. HAADF-STEM images (High-angle annular dark-field imaging scanning transmission electron microscopy) of **b)** fully deactivated and **d)** reactivated $20CeO_2@ZrO_2$. **e)** XEDS maps of overlap of Ce (blue) and Zr (green) of fully reactivated $20CeO_2@ZrO_2$. XEDS maps show the distribution of Ce, Zr and Cl.

In order to demonstrate the high sensitivity of the present UV-Vis based reactor experiment we investigated the chlorination degree of stable $CeO_2$-based catalysts that have not suffered from bulk chlorination (cf. Figure 6). The integral chlorine intensities in the dechlorination peaks and the BET surface areas of $CeO_2$ and $20CeO_2@ZrO_2$ are practically identical (cf. Figure 6). This observation points to a similar chemical nature of the active phases. The amount of chlorine accommodated at the surface of the $CeO_2$ particle can be determined from these experiments. It turns out that the chlorination degree of pure $CeO_2$ is about 10%, while that of $20CeO_2@ZrO_2$ is 30%. The former value for pure $CeO_2$ agrees surprisingly well with the PGAA-derived value of about 10% reported in the literature.[13]

For the case of pure $CeO_2$ with a BET surface area of maximum $46 \pm 2\ m^2/g$ (Table 1: fresh sample, BET surface decreases slightly upon Deacon reaction) and 30 mg catalyst, the total surface area is 1.38 $m^2$. From surface science experiments we know that the density of surface chlorine on $CeO_2(111)$ is at least 1Cl atom/1.38 $nm^2$ but not more than 2Cl atoms/1.38 $nm^2$.[25] The upper limit is therefore $1.46 \cdot 10^{17}$ surface Cl atoms that corresponds to a maximum degree of chlorination of 0.8%. From this estimation we conclude that the found degree of chlorination of 10% corresponds to much more chlorine at $CeO_2$ than just realized by adsorbed chlorine on the surface.

### 2.3. Kinetics of the reoxidation process

We show experimentally that the fully and partially chlorinated $CeO_2$ and $20CeO_2@ZrO_2$ catalysts can be reoxidized and therefore be reactivated by exposure to oxygen. We observe substantial differences between the studied catalysts regarding both the shape of the evolved chlorine signal, and the overall kinetics of the reoxidation process. The overall kinetics can be

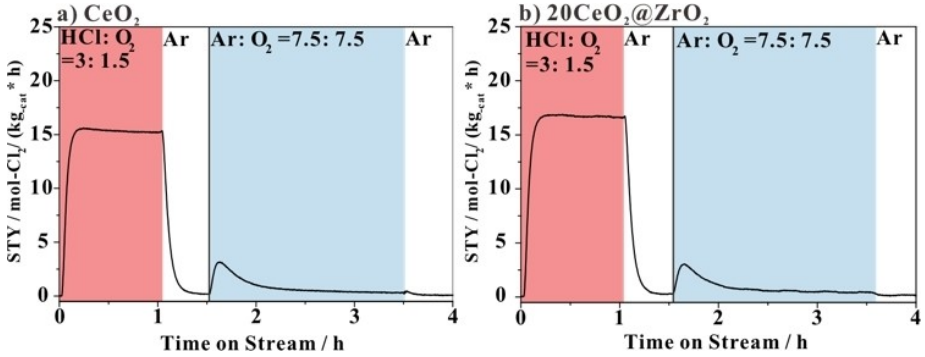


**Figure 6.** Chlorine evolution of a) pure $CeO_2$ and b) 20 mol% $CeO_2$ supported on $ZrO_2$ ($20CeO_2@ZrO_2$) under the HCl oxidation reaction at $T = 430\,^{\circ}C$, total flow rate15 sccm, 30 mg catalyst as a function of time on stream under varying reaction conditions: first the reaction mixture was $Ar:HCl:O_2 = 10.5:3:1.5$ and then it was switched to $Ar:HCl:O_2 = 7.5:0:7.5$.

described by the reaction half time $t_{1/2}$, at which half the material has reacted. For the pure $CeO_2$ sample we obtain a $t_{1/2}$ of 0.52 h and 0.55 h for the first and second reoxidation. For $20CeO_2@ZrO_2$ we obtain 0.12 h for both reoxidation experiments. Moreover, we observe different shapes of the evolved chlorine signal during the reoxidation of the two samples. We employ the phenomenological model described in Experimental Section for the modelling of the experimental data.

For the reoxidation of the supported catalyst $20CeO_2@ZrO_2$ we assume that most $CeO_2$ is formed in particle shape, and that the $CeO_2$ film supported on the $ZrO_2$ particles is negligible in a first approximation, since the reoxidation experiment measures the total $Cl_2$ evolved in the reoxidation of both the active film and the less active particle, and 75% of the $CeO_2$ assumes the form of particles in the fresh catalyst. However, we note that the highly dispersed $CeO_2$ film dominates the catalytic activity of $20CeO_2@ZrO_2$ in the HCl oxidation. We further assume that the growth of the $CeO_2$ particles in the pure $CeO_2$ and $20CeO_2@ZrO_2$ catalysts can be described by the same reaction order $m$ and rate constant for growth $k_{grow}$. However, we expect nucleation to be different in the two samples, using two different parameters $k_{nuc,CeO_2}$ and $k_{nuc,CeO_2@ZrO_2}$ that reflect the absence and presence of the $ZrO_2$ support. We therefore employ four parameters, $m$, $k_{grow}$, $k_{nuc,CeO_2}$ and $k_{nuc,CeO_2@ZrO_2}$, to model all four reoxidation experiments of the completely chlorinated samples (Figures 2, 3).

Since the supported catalyst is expected to exhibit two different growth modes (layer and particle), but our model only describes one growth mode (particle), we expect larger deviations for the supported catalyst. In order to avoid meaningless fit results, we assign the $20CeO_2@ZrO_2$ catalyst a lower weight, which results in better fit of the $CeO_2$ reoxidation signal. The weights are 1 and 0.5 for the reoxidation of pure $CeO_2$ and $20CeO_2@ZrO_2$.

While we employ the same reaction order and rate constants to describe the growth both in the pure and supported catalysts, we realize that the samples differ in several ways; for instance, the pure $CeO_2$ catalyst is not completely oxidized, which possibly influences the reoxidation kinetics.

Our model takes into consideration the state of the deactivated sample through the boundary conditions $r(0)$ (particle radius) and $\varepsilon_{CeO_2}(0)$ (volume fraction of residual $CeO_2$). The boundary conditions for $r(0)$ and $\varepsilon_{CeO_2}(0)$ for the pure $CeO_2$ catalyst are chosen based on the experimental result that only 75% of the sample has been chlorinated, that is, $\varepsilon_{CeO_2}(0) = 0.25$. The starting radius of the nuclei is taken from the Rietveld refinement (19 nm). The boundary conditions for the second reoxidation experiment are obtained in similar fashion as listed in Table 3. For the $20CeO_2@ZrO_2$ catalyst, we observe that the first chlorination is complete, so both $\varepsilon_{CeO_2}(0)$ and $r(0)$ are zero. For the second reoxidation experiment, $\varepsilon_{CeO_2}(0) = 0.09$. We have no data on the residual $CeO_2$ particle radius, so that we chose $r(0) = 5$ nm, slightly smaller than the particle size after reoxidation (7.8 nm). We note that the model results are insensitive to the choice of the initial particle radius for $r(0) < 30$ nm due to the high growth rate obtained in the model fit.

**Table 3.** Boundary conditions and weights for the kinetic model as obtained from experimental catalyst characterization.

| Sample | cycle | $\varepsilon_{CeO_2}(0)$ | $r(0)$ [nm] | $w$ |
|---|---|---|---|---|
| $CeO_2$ | 1st | 0.24 | 19 | 1 |
| $CeO_2$ | 2nd | 0.32 | 19 | 1 |
| $20CeO_2@ZrO_2$ | 1st | 0 | 0 | 0.5 |
| $20CeO_2@ZrO_2$ | 2nd | 0.09 | 5 | 0.5 |

**Table 4.** Fitted parameters for the reoxidation model.

| Parameter | Fitted value |
|---|---|
| $m$ | 1.01 |
| $k_{grow}$ | 50.9 nm $(h\,bar)^{-1}$ |
| $k_{nuc,CeO_2}$ | 5.89 $(h\,nm^3\,bar)^{-1}$ |
| $k_{nuc,CeO_2@ZrO_2}$ | 192.9 $(h\,nm^3\,bar)^{-1}$ |

The parameters $m$, $k_{grow}$, $k_{nuc,CeO_2}$ and $k_{nuc,CeO_2@ZrO_2}$ are fitted by minimizing $\bar{S}$ through recursive parameter sweeping. The fitting results are given in Table 4. The fitted chlorine signals are displayed as a function of time in Figure 7. The agreement between model and experiment is quite good for both reoxidation cycles of pure $CeO_2$ (Figure 7a), as well as for the second reoxidation cycle of the supported catalyst (Figure 7b). For the first reoxidation cycle we observe a higher signal intensity, as well as a slow decay of the signal that our model is unable to reproduce. However, our model can describe the overall rate and reaction half time of the reoxidation reaction quite well, resulting in a faster reoxidation of the supported catalyst compared to the pure catalyst. Since our model assumes that the $CeO_2$ growth rate (50.9 nm $(h\,bar)^{-1}$) is unaffected by the presence of $ZrO_2$, the difference in the reoxidation kinetics is traced to a nucleation rate in the supported catalyst (192.9 $(h\,nm^3\,bar)^{-1}$) that is a factor of 32 higher than in the pure $CeO_2$ catalyst (5.89 $(h\,nm^3\,bar)^{-1}$). While $ZrO_2$ itself is inert in the chlorination and reoxidation reaction, it can provide surface area where $CeO_2$ particles can nucleate, thereby accelerating the overall reoxidation reaction. Furthermore, we know from TEM imaging (Figure 5c, d) that the $CeCl_3$ particles are well-dispersed over the $ZrO_2$ surface, contributing to the high observed nucleation rate. While the overall nucleation rates seem similar, we emphasize that the resulting kinetics drastically differ for the two samples, which means that the experiment is highly sensitive to the nucleation rate. The high nucleation rate in the supported sample can be interpreted as the preference to form new $CeO_2$ particle presumably on the $ZrO_2$ surface over the growth of existing $CeO_2$ particles. This can possibly prevent the ripening of $CeO_2$ particles in successive reduction-oxidation cycles and can be relevant for the long-term stability of the catalyst.

## 3. Discussion

How does our approach compare with other methods for quantifying the degree of chlorination? So far, mostly Rietveld

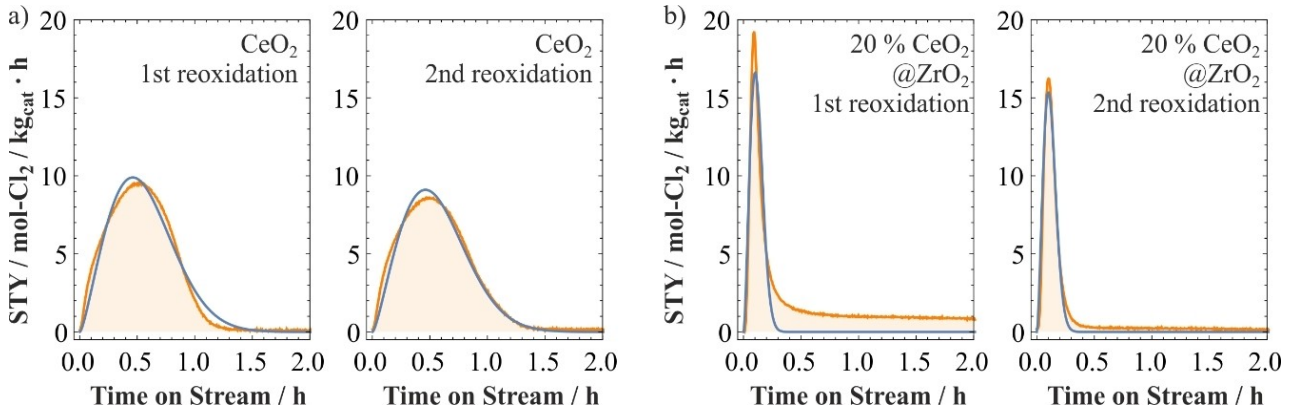


**Figure 7.** Modeled chlorine evolution curves during reoxidation (blue) employing the model described in Section 2.2 and the boundary conditions and fitted parameters in Tables 3 and 4. Experimentally measured curves are displayed in orange.

analyses of XRD data have been employed to quantify the bulk chlorination of $CeO_2$-based catalysts.[10,11] This method is only applicable if hydrated $CeCl_3$ is crystalline. Fortunately, this happens to be the case for fully deactivated $CeO_2$-samples, although the X-ray amorphous part is unknown. However, XRD is not applicable for determining the degree of chlorination of a stable catalyst. Here, X-ray photoemission spectroscopy (XPS) can estimate the degree of chlorination of a stable $CeO_2$-based catalyst, although this method is not quantitative. From previous XPS studies, there is evidence that the chlorination degree is higher than just a surface coverage of chlorine for pure $CeO_2$ would presume.[9] TGA together with mass spectrometry can be utilized for quantifying the degree of chlorination without relying on crystallinity of the chloride.[8] However, all three methods suffer from being ex-situ in that the chlorinated catalyst has to be removed from the reactor in order to quantify its degree of chlorination.

Prompt Gamma Activation Analysis (PGAA) is particularly useful for the quantification of the chlorination degree since it can work even under reaction conditions or at least *in situ* in the reactor. PGAA has mostly been employed for biological systems,[27] albeit it is not restricted to such systems. PGAA is quantitative and sensitive, but it requires a neutron source that rules out this method for standard analysis. Both Ce and Cl concentration can be determined separately and therefore the molar ratio Cl/Ce.[28] The uncertainties for quantifying the degree of chlorination are small so that even differences in chlorination degree of the catalysts of a few mol% as a function of the reaction mixture can be determined.[13] The drawback of PGAA is its relatively long data acquisition time (typically 1–2 h time) so that the kinetics of the reoxidation process during reactivation is not accessible.

The present *in situ* approach using UV-Vis detection in the Deacon reactor is fast and sensitive (ca. 1/10 monolayer), so that it is able to resolve the kinetics of the reoxidation step. Our approach is however not operando, since it requires a switch of the reaction mixture. Therefore, firm conclusions about the active phase cannot be drawn, although conclusions about the reactivation process of the catalysts are clear-cut.

It has been recognized that $CeO_2$-based catalysts deactivate in the Deacon reaction through bulk chlorination.[8,9,11] There is also clear evidence that stoichiometric CeOCl is catalytically not active at all.[14] Figure 8 summarizes the chlorination and oxidation of the pure (top) and supported catalysts (bottom) in a scheme. The deactivation of pure $CeO_2$ (top) leads to 70% chlorination, but the catalyst can be reactivated under reaction conditions with excess oxygen in the reaction feed at reaction temperatures of typically 430 °C.[8,13] Here we show that the restoration of bulk-chlorinated $CeO_2$ is almost quantitative. Through quantification of the reoxidation peak during the first reactivation cycle of deactivated $CeO_2$, we obtained a chlorination degree of 77%. A very similar value was determined by Rietveld refinement of XRD patterns for the deactivated $CeO_2$, namely 76%. The coexistence of hydrated $CeCl_3$ and $CeO_2$ in deactivated $CeO_2$ can equally be verified by the Raman spectroscopy and XPS. This finding can possibly be explained by $CeCl_3$ particles blocking the surfaces of $CeO_2$ as indicated in Figure 8 (top), thereby preventing further chlorination. Subsequently, we evaluated the catalytic activity of reactivated $CeO_2$ under the mild Deacon condition. The activity of reactivated $CeO_2$ is 17% lower than that of the fresh one. From XRD it is evident that the $CeO_2$ particles have significantly grown in size after reactivation. Particles with smaller initial size may have disappeared more quickly upon chlorination than larger particles as indicated in Figure 8. Upon reoxidation, the growth of residual oxide particles is kinetically favored over nucleation of new particles, consistent with the low nucleation rate obtained in fitting the experimental reoxidation kinetics. The increase of the $CeO_2$ particle size concomitant with a smaller active surface area could be the reason for the observed decline in the steady state activity of $CeO_2$. The quantification of the second reoxidation peak yields a chlorination degree of 72%. The decline of the chlorination degree compared to the first time (77%) is rationalized by the growth of larger $CeO_2$ particles that are less prone to be chlorinated. The catalytic activity of $CeO_2$ after the second reactivation is 6% lower than after the first reactivation. This finding suggests that the deactivation/

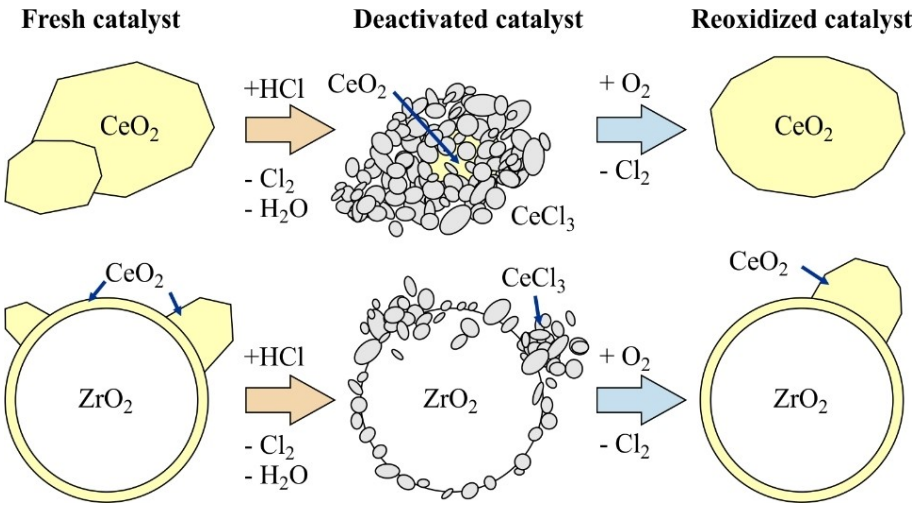


**Figure 8.** Scheme of chlorination and reoxidation and subsequent particle agglomeration for the pure $CeO_2$ catalyst (top) and the supported $CeO_2$@$ZrO_2$ catalyst (bottom).

reactivation process facilitates progressive sintering of the active component $CeO_2$.

So far, no reactivation experiments for 20$CeO_2$@$ZrO_2$ have been reported. From the first reoxidation $Cl_2$ peak of deactivated $CeO_2$ (Figure 3) we determine the chlorination degree of 20$CeO_2$@$ZrO_2$ to be 100%, i.e., all $CeO_2$ is transformed to hydrated $CeCl_3$, consistent with Rietveld refinement of corresponding XRD data. The Raman spectrum and XPS of deactivated 20$CeO_2$@$ZrO_2$ agree that the active ceria component in 20$CeO_2$@$ZrO_2$ is fully chlorinated. As observed in TEM images of the deactivated catalyst (Figures 5a, b), the $CeCl_3$ phase is dispersed over the $ZrO_2$ surface as indicated in Figure 8 (bottom). Moreover, the reactivation of 20$CeO_2$@$ZrO_2$ proceeds substantially faster than for pure $CeO_2$ due to the fine $CeCl_3$ dispersion and high nucleation rate of $CeO_2$ on the support surface. The activity of the 20$CeO_2$@$ZrO_2$ sample after the first reactivation is only 8% lower than that of the fresh one. From the XRD experiments we know that during the first cycle the attached $CeO_2$ particles grow in size (XRD) consistent with a stronger ceria peak intensity in the Raman spectrum. TEM reveals that the $CeO_2$ wetting layer is fully recovered after reactivation (Figure 5c, d) and takes over most of the catalytically active phase. After the second deactivation step, the chlorination degree is only 91%, which can be attributed to the increase of the $CeO_2$ particle size as also reconciled with the Rietveld refinement. After the second reactivation step the sample recovers 99% of its catalytic activity. Therefore, we infer that the activity of the 20$CeO_2$@$ZrO_2$ catalyst will be stable and not reduced after further "deactivation-reactivation" cycles.

In order to understand the restoration of the 20$CeO_2$@$ZrO_2$ morphology and the full recovery of the activity after reactivation, we presume that the formed $CeCl_3 \times nH_2O$ particles need to adhere to the $ZrO_2$ support with high dispersion. This presumption is confirmed by TEM images (cf. Figures 5c, d). When subsequently the deactivated 20$CeO_2$@$ZrO_2$ catalyst is exposed to oxygen, the adhering $CeCl_3 \times nH_2O$ layer transforms back to a thin covering layer of $CeO_2$ on $ZrO_2$ without significantly changing the morphology. The constraint of $CeCl_3 \times 6H_2O$ adhering to the $ZrO_2$ surface restricts the mass transport to surface diffusion on the $ZrO_2$ surface and keeps the active surface area of exposed $CeO_2$ constant after reactivation.

It is evident that reactivation for pure $CeO_2$ takes much longer than that for 20 mol% $CeO_2$ supported on $ZrO_2$ (cf. Figure 9). In addition, we observe different shapes of the $Cl_2$ signals during reoxidation. For a more quantitative description, we employ a phenomenological model based on the JMAK approach where a phase transformation is modeled by a nucleation and growth mechanism. In addition, we need to take into account the different starting conditions in the two samples. Fitting different parameters for the nucleation rates for pure $CeO_2$ and 20$CeO_2$@$ZrO_2$ results in a nucleation rate that is 32 times higher for 20$CeO_2$@$ZrO_2$. The result can be explained by the high initial dispersion of $CeCl_3$ and the inert $ZrO_2$ surface providing nucleation sites for the growth of $CeO_2$. While only 75% of the catalyst is chlorinated in the pure $CeO_2$ samples, the fitted nucleation rate is substantially lower, possibly indicating

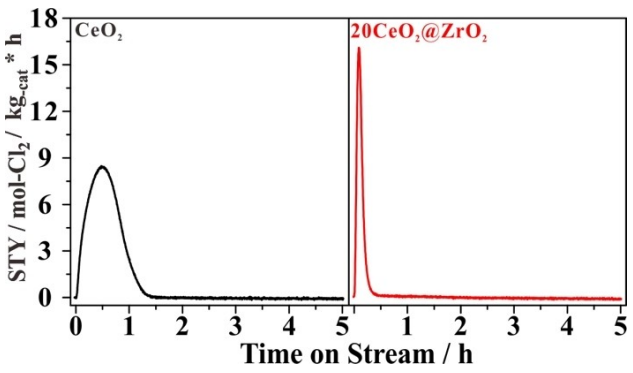


**Figure 9.** Time needed for reactivation of $CeO_2$ in comparison to that of 20$CeO_2$@$ZrO_2$ after the activity measurement of fully-deactivated state.

that the $CeO_2$ surface contributes less to nucleation. This assumption is consistent with the earlier conclusion that the surface of residual $CeO_2$ is entirely covered by $CeCl_3$ after chlorination (and thereby not available as a site for oxide nucleation), thereby suppressing complete chlorination.[11]

Finally, we raise the question why the $CeO_2$ layer on $ZrO_2$ is always restored during reoxidation. While higher stability of the $CeO_2$ film grown on $ZrO_2$ compared to $CeO_2$ particles may be one possible explanation for the reversible film restoration, we currently have no insight into the relative (thermodynamic) stabilities of the $CeO_2$ film on $ZrO_2$ versus $CeO_2$ bulk particles. However, our fitted nucleation rate constants suggest that nucleation appears to be faster when the $ZrO_2$ surface is exposed. The support surface may thereby aid in the redispersion of the catalyst upon reoxidation.

Our kinetic model for the reoxidation could be further refined by considering additional steps of the reaction and different nucleation sites and growth modes of the formed $CeO_2$ films and particles, for instance, in the form of a Kinetic Monte Carlo model;[29] however, we cannot meaningfully fit more parameters to the available data. More detailed models to obtain deeper understanding of catalyst degradation and reactivation needs extended experimental data sets under various reaction conditions or a first-principles-based approach.

The deactivation/reactivation cycle of $CeO_2$ based catalysts in the HCl oxidation reaction can be considered as a redox reaction where the reduction and oxidation step is separated (similar to an electrochemical reaction). Actually in this kind of Born-Haber cycle, chlorine can be produced within a cycle of solid state reactions: metal oxide is chlorinated first to form metal chloride (exothermic) and then in a separate chamber the metal chloride is reoxidized (endothermic) to release the desired product $Cl_2$ and to recover the metal oxide.[4,6] Therefore, we can ask ourselves how important is the chlorine release in the reoxidation of the $CeO_2$-based catalyst for the overall conversion of HCl. For the active and stable catalyst, there is only little chlorine at the surface. The replacement of this chlorine species by oxygen amounts only to about 20% of the reached rate under steady state Deacon conditions (cf. Figure 6). Therefore, this contribution is likely to be not relevant for the overall conversion, although it is important for the chemical nature of the catalytically active phase.

## 4. Conclusion

Pure $CeO_2$ and 20 mol% $CeO_2$ supported on preformed $ZrO_2$ particles ($20CeO_2@ZrO_2$) fully deactivate under harsh HCl oxidation conditions by the formation of Ce bulk chlorides. With an oxidative step in a pure oxygen atmosphere the deactivated catalysts can be reactivated by reoxidation and the replaced chlorine can be quantified in-situ by the UV-Vis analytics in the flow reactor. The catalytic activity of $20CeO_2@ZrO_2$ is completely recovered after the second deactivation/reactivation cycle, while the activity of pure $CeO_2$ after reactivation declines steadily. UV-Vis data acquisition is fast so that the kinetics of the reactivation step via the reoxidation can readily be followed and be used to model the solid-state reaction mechanism of the dechlorination reaction of hydrated $CeCl_3$ by oxygen. With a simple nucleation and growth model based on the JMAK approach, the different reoxidation kinetics of the two samples can be explained by high nucleation rate of $CeO_2$ on the $ZrO_2$ support surface. While the $ZrO_2$ surface is otherwise inert in the HCl oxidation reaction, it appears to provide sites for the nucleation of $CeO_2$ particles and keeps $CeCl_3$ particles in the chlorinated catalyst dispersed. The $ZrO_2$ support thereby aids in the redispersion of the catalyst during chlorination-dechlorination cycles. We conclude that the choice of catalyst support is crucial to prevent catalyst deactivation in non-steady-state operation.

The UV-Vis analytics is very sensitive so that even the chlorination degree of stable catalysts can be quantified with values that are in close agreement with those derived from PGAA experiments. The chlorination degree of stable catalysts is significantly higher than expected from a bare Cl overlayer with severe consequences for the reaction mechanism and hence for its theoretical modeling.

We propose that *in-situ* deactivation and reactivation experiments, coupled with an accurate quantification of the degree of transformation and theoretical modeling can be used to gain a detailed understanding of how the support alters the stability and activity of catalyst required to further improve catalyst-support combinations. In principle, this kind of in-situ experiments can be employed whenever the product or the educt is able to transform the chemical (bulk) composition of catalyst, thus opening the door for further experiments and scientific questions.[30]

## Author contribution

Y. Sun prepared the materials and conducted the experiments and wrote a first draft. F. Hess developed the reoxidation model and performed the theoretical analysis. I. Djerdj performed the Rietveld analysis. T. Weber conducted the XPS experiments and analyzed the XPS data; Zhen Wang performed some of the activity experiments. H. Over conceived the original idea and took the lead in writing the manuscript with contributions from Y. Sun, F. Hess, and Bernd Smarsly.

## *Acknowledgements*

*This work was supported by the National Key Research and Development Program of China (2016YFC0204300), National Natural Science Foundation of China (21577035), Commission of Science and Technology of Shanghai Municipality (13521103402, 15DZ1205305) and 111 Project (B08021). Yu Sun gratefully acknowledge the China Scholarship Council for the Joint-Ph.D program between the Research Institute of Industrial Catalysis of East China University of Science and Technology and the Physical Chemistry Institute of Justus-Liebig-University Giessen. We acknowledge support from the Laboratory of Materials Research at the JLU. Franziska Hess acknowledges funding by Fond der*

*Chemischen Industrie in the form of a Liebig fellowship (Li 204/02). Open access funding enabled and organized by Projekt DEAL.*

## *Conflict of Interest*

The authors declare no conflict of interest.

**Keywords:** Deacon reaction · stability · reactivation · *in situ* experiment · Avrami modelling

[1] S. L. Scott, *ACS Catal.* **2018**, 8, 8597–8599.
[2] M. D. Argyle, C. H. Bartholomew, *Catalysts* **2015**, *5*, 145–269.
[3] J. Pérez-Ramírez, C. Mondelli, T. Schmidt, O. F. K. Schlüter, A. Wolf, L. Mleczko, T. Dreier, *Energy Environ. Sci.* **2011**, *4*, 4786–4799.
[4] H. Over, R. Schomäcker, *ACS Catal.* **2013**, *3*, 1034–1046.
[5] K. Seki, *Catal. Surv. Asia* **2010**, *14*, 168–175.
[6] M. W. M. Hisham, S. W. Benson, *J. Phys. Chem.* **1995**, *99*, 6194–6198.
[7] D. Crihan, M. Knapp, S. Zweidingey, E. Lundgren, C. J. Weststrate, J. N. Andersen, A. P. Seitsonen, H. Over, *Angew. Chem. Int. Ed.* **2008**, *47*, 2131–2134; *Angew. Chem.* **2008**, *120*, 2161–2164.
[8] A. P. Amrute, C. Mondelli, M. Moser, G. Novell-Leruth, N. López, D. Rosenthal, R. Farra, M. E. Schuster, D. Teschner, T. Schmidt, J. Pérez-Ramírez, *J. Catal.* **2012**, *286*, 287–297.
[9] C. Li, Y. Sun, I. Djerdj, P. Voepel, C. Sack, T. Weller, R. Ellinghaus, J. Sann, Y. Guo, B. M. Smarsly, H. Over, *ACS Catal.* **2017**, *7*, 6453–6463.
[10] C. Li, F. Hess, I. Djerdj, G. Chai, Y. Sun, Y. Guo, B. M. Smarsly, H. Over, *J. Catal.* **2018**, *357*, 257–262.
[11] C. Li, Y. Sun, F. Hess, I. Djerdj, J. Sann, P. Voepel, P. Cop, Y. Guo, B. M. Smarsly, H. Over, *Appl. Catal. B* **2018**, *239*, 628–635.
[12] R. Lin, A. P. Amrute, J. Pérez-Ramírez, *Chem. Rev.* **2017**, *117*, 4182–4247.
[13] R. Farra, M. Eichelbaum, R. Schlögl, L. Szentmiklósi, T. Schmidt, A. P. Amrute, C. Mondelli, J. Pérez-Ramírez, D. Teschner, *J. Catal.* **2013**, *297*, 119–127.
[14] Farra, F. Girgsdies, W. Frandsen, M. Hashagen, R. Schlögl, R. Teschner, *Catal. Lett.* **2013**, *143*, 1012–1017.
[15] S. Urban, N. Tarabanko, C. H. Kanzler, K. Zalewska-Wierzbicka, R. Ellinghaus, S. F. Rohrlack, L. Chen, P. J. Klar, B. M. Smarsly, H. Over, *Catal. Lett.* **2013**, *143*, 1362–1367.
[16] Y. Sun, C. Li, I. Djerdj, O. Khalid, P. Cop, J. Sann, T. Weber, S. Werner, K. Turke, Y. Guo, B. M. Smarsly, H. Over, *Catal. Sci. Technol.* **2019**, *9*, 2163–2172.
[17] M. Moser, C. Mondelli, T. Schmidt, F. Girgsdies, M. E. Schuster, R. Farra, L. Szentmiklósi, D. Teschner, J. Pérez-Ramírez, *Appl. Catal. B* **2013**, *132–133*, 123–131.
[18] Y. Sun, P. Cop, I. Djerdj, X. Guo, T. Weber, O. Khalid, Y. Guo, B. M. Smarsly, H. Over, *ACS Catal.* **2019**, *9*, 10680–10693.
[19] R. Farra, M. Garcia-Melchor, M. Eichelbaum, M. Hashagen, W. Frandsen, J. Allan, F. Girgsdies, L. Szentmiklosi, N. Lopez, *ACS Catal.* **2013**, *3*, 2256–2268.
[20] C. H. Kanzler, S. Urban, K. Zalewska-Wierzbicka, F. Hess, S. F. Rohrlack, C. Wessel, R. Ostermann, J. P. Hofmann, B. M. Smarsly, H. Over, *ChemCatChem* **2013**, *5*, 2621–2626.
[21] P. Fornasiero, G. Balducci, R. Di Monte, J. Kašpar, V. Sergo, G. Gubitosa, A. Ferrero, M. Graziani, *J. Catal.* **1996**, *164*, 173–183.
[22] Q. Xie, H. Zhang, J. Kang, J. Cheng, Q. Zhang, Y. Wang, *ACS Catal.* **2018**, *8*, 4902–4916.
[23] P. Burroughs, A. Hamnett, A. F. Orchard, G. Thornton, *J. Chem. Soc. Dalton Trans.* **1976**, *17*, 1686–1698.
[24] S. Suzuki Takehiko Ishii, T. Sagawa, *J. Phys. Soc. Jpn.* **1974**, *37*, 1334–1340.
[25] C. Sack, P. Lustemberg, V. Koller, V. Ganduglia-Priovano, H. Over, *J. Phys. Chem. C* **2018**, *122*, 19584–19592.
[26] J. W. Christian, *Formal Theory of Transformation Kinetics*, (Eds.: J. W. Christian), Pergamon, Oxford, **2002**, pp. 529–552.
[27] Zs. Révay, T. Belgya, L. Szentmiklósi, Z. Kis, A. Wootsch, D. Teschner, M. Swoboda, R. Schlögl, J. Borsodi, R. Zepernick, *Anal. Chem.* **2008**, *80*, 6066–6071.
[28] D. Teschner, R. Farra, L. Yao, R. Schlögl, H. Soertjanto, R. Schomäcker, T. Schmidt, L. Szentmiklósi, A. P. Amrute, C. Mondelli, J. Pérez-Ramírez, G. Novell-Leruth, N. López, *J. Catal.* **2012**, *285*, 273–284.
[29] V. P. Zhdanov, *Surf. Rev. Lett.* **2008**, *15*, 605–612.
[30] R. Schlögl, *Angew. Chem. Int. Ed.* **2015**, *54*, 3465–3520; *Angew. Chem.* **2015**, *127*, 3531–3589.

Manuscript received: May 29, 2020
Revised manuscript received: July 2, 2020
Accepted manuscript online: July 10, 2020
Version of record online: September 9, 2020